Groundwater controls on colloidal transport in forest stream waters

N. Gottselig[a], J. Sohrt[b], D. Uhlig[c,d], V. Nischwitz[e], M. Weiler[b], W. Amelung[a,d]*

[a]Institute of Crop Science and Resource Conservation, Soil Science and Soil Ecology, University of Bonn, Nussallee 13, 53115 Bonn, Germany

[b]Chair of Hydrology, Albert-Ludwigs-Universität Freiburg, Friedrichstraße 39, 79098 Freiburg, Germany

[c]GFZ German Research Centre for Geosciences, Section Earth Surface Geochemistry, Telegrafenberg, 14473 Potsdam, Germany

[d]Forschungszentrum Jülich GmbH, Institute of Bio- and Geosciences, IBG-3: Agrosphere, 52425 Jülich, Germany

[e]Forschungszentrum Jülich GmbH, Central Institute for Engineering, Electronics and Analytics (ZEA-3), 52425 Jülich, Germany

*: Corresponding author; email: ngottsel@uni-bonn.de
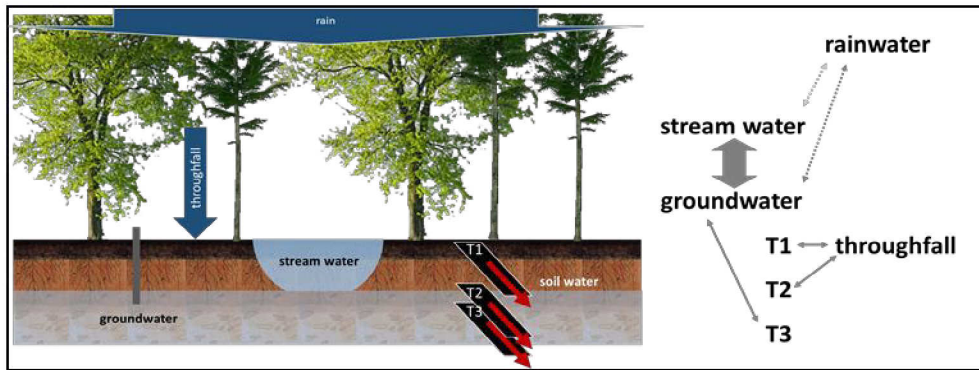
Highlights:

- The origin of colloids in streams indicates elemental transport pathways.
- Monthly analysis of stream & groundwater, rainwater, throughfall, soil leachate.
- Field flow fractionation revealed three fractions in all sample types.
- Groundwater derived colloids dominated the stream signal.
- Water flux and particle reformation affect the seasonal dynamics of particles.

1   *Abstract*

2   Biogeochemical changes of whole catchments may, at least in part, be deduced from changes

3   in stream water composition. We hypothesized that there are seasonal variations of natural

4   nanoparticles (NNP; 1-100 nm) and fine colloids (<300 nm) in stream water, which differ in

5   origin depending on catchment inflow parameters. To test this hypothesis, we assessed the

6   annual dynamics of the elemental composition of NNP and fine colloids in multiple water

7   compartments, namely in stream water, above and below canopy precipitation, groundwater

8   and lateral subsurface flow from the Conventwald catchment, Germany. In doing so, we

9   monitored meteorological and hydrological parameters, total element loads, and analyzed

10   element concentrations of org C, Al, Si, P, Ca, Mn and Fe by Asymmetric Flow Field Flow

11   Fractionation (AF[4]). The results showed that colloid element concentrations were <5 µmol/L.

12   Surprisingly, up to an average of 55 % (Fe) of total element concentrations were not truly

13   dissolved but bound to NNP and fine colloids. The colloid patterns showed seasonal variability

14   with highest loads in winter. The presence of groundwater-derived colloidal Ca in stream

15   water showed that groundwater mainly fed the streams throughout the whole year. Overall,

16   the results showed that different water compartments vary in the NNP and fine colloidal

17   composition making them a suitable tool to identify the streams NNP and fine colloid sources.

18   Given the completeness of the dataset with respect to NNP and fine colloids in multiple water

19   compartments of a single forest watershed this study adds to the hitherto underexplored role

20   of NNP and fine colloids in natural forest watersheds.

21

1. Introduction

Forest ecosystems critically link the earth's water and nutrient cycles, making them vital components of the global ecosystem (Perry et al., 2008). Therefore, studying pristine forests may provide a benchmark for the natural cycling of elements in terrestrial environments. The element loss from such an ecosystem is largely reflected by the element load in stream waters. Frequently, samples are filtered to gain an operationally defined dissolved phase (<0.45 µm) of elements. This definition, however, takes the risk of including very fine particles in the size range of natural colloids (1 nm-1 µm), specifically of nanoparticles (NNP, 1-100 nm), the presence of which may alter the bioavailability of the elements and thus subsequent interpretations from studying stream water composition. The consideration of colloids and especially NNP is highly relevant as up to 90-100% of the elements Fe, P, Mn, Al and organic carbon (org C), for instance, have been detected in the specific size range of NNP and colloids and not in dissolved state (Baalousha et al., 2011; Baken et al., 2016b; Gottselig et al., 2017a; Jarvie et al., 2012; Missong et al., 2018a). To understand the processes governing the biogeochemical cycling of elements in forested watersheds, a prerequisite is to link NNP and colloid mediated transport/export with hydrological processes determining the flow of the particle transport medium water.

As a subset of colloids, NNP are of particular interest as elemental carrier due to their higher specific surface area in comparison to larger sized colloids or particles (Hartland et al., 2013). The reactivity of NNP renders them potentially predominant carriers of limiting nutrients such as P in headwater catchments. Fundamental building blocks of NNP in acidic freshwaters and carriers of multiple further elements are most frequently Fe and/or org C (Andersson et al., 2006; Neubauer et al., 2013), and clay minerals in the fine colloidal size range (100-450 nm) (Gottselig et al., 2017b; Hill and Aplin, 2001; Missong et al., 2018b). In so far as the chemical

2

46   composition of these particles is preserved during transport within the catchment, it can be

47   used as an indicator of the potential origin of the stream's NNP and colloids. For this purpose,

48   NNP and colloids must be analyzed from the entirety of water compartments contributing to

49   the stream, i.e., in rainwater and throughfall, as well as in lateral subsurface flow, ground- and

50   stream water.

51   To our knowledge there is only one single study of NNP and colloids in rainwater and

52   throughfall from Gandois et al. (2010). They assigned an important role to local atmospheric

53   emissions for the composition of rainwater particles, whereas dry deposition and canopy

54   leaching modified the chemical composition of particles carried by throughfall. Gandois et al.

55   (2010) additionally reported that complexation with organic matter promoted formation and

56   dissolution of colloids in throughfall; specifically Al, Fe and Pb were found associated to org C.

57   Yet, Gandois et al. (2010) restricted their analysis to bulk deposition and throughfall samples

58   collected weekly over one year and, therefore, could not compare their data to soil, stream or

59   groundwater of the same catchment.

60   In contrast to precipitation waters, NNP and colloids dispersed or leached from soil are usually

61   substantially higher concentrated and likely exhibit a more diverse elemental composition.

62   Missong et al. (2018b) attempted a first comparison between colloids from soil leachates

63   (Missong et al., 2018b), soil extracts (Missong et al., 2018a) and stream water colloids

64   (Gottselig et al., 2017b) of the same sites and found a close similarity between stream water

65   and soil leachate NNP and colloids. A common feature of all three sample types was the

66   detection of an org C-rich NNP fraction <20-25 nm, which also contains Fe, Al, Mn, Ca and P;

67   as also reported by other studies (Baken et al., 2016b; Gottselig et al., 2014; Gottselig et al.,

68   2017b; Haygarth et al., 1997; Jiang et al., 2015; Regelink et al., 2013; Regelink et al., 2014).

69   The chemical composition of NNP between 20/25 nm to 60/70 nm matches between stream

70 waters and soil leachates, showing dominant concentrations of org C, Fe, Al and P (Gottselig

71 et al., 2017b; Missong et al., 2018b), but these fractions can also contain substantial amounts

72 of Ca and Mn (Gottselig et al., 2017a). Extracted soil particles 25-240 nm were dominated by

73 Fe (Missong et al., 2018a) and potentially include instable, artificially mobilized particles

74 (Missong et al., 2018b) that are either filtered or decay and thus likely do not reach the

75 streams or groundwater bodies. Particles extracted from soil usually exhibited a wider size

76 range of particles (up to 500 nm) than streams or leachates (up to 300-400 nm). It is therefore

77 necessary to elucidate the presence of colloid fractions in all water compartments within a

78 forested watershed to deduce conclusions on intercompartment mobility.

79 Nanoparticle transport at saturated flow may reach the groundwater if colloid phase stability

80 is given (Degueldre et al., 2000) and when the topsoil is hydraulically connected to

81 groundwater at moist conditions. Studies on the elemental presence in groundwater agree

82 that the composition of the bedrock surrounding the aquifer dominates the general elemental

83 composition found in the groundwater (e.g. Rosenthal, 1987). The same is also valid for

84 potentially present colloids (Degueldre et al., 2000). Surprisingly, data on groundwater

85 colloids is scarce (Baalousha et al., 2011). The studies of Cizdziel et al. (2008) and Baik et al.

86 (2007) have identified NNP in groundwater but also larger sized colloids containing a variety

87 of elements. Saito et al. (2015) compared the chemical composition of colloids in groundwater

88 draining sedimentary and granitic bedrock and also found some larger inorganic colloids.

89 Despite low concentrations, NNP fractions <10 nm dominated mass fluxes for both

90 groundwater aquifers. The exact origin of the NNP remained open.

91 Through temporal imbalances of recharge and drainage, most groundwater bodies display a

92 seasonally fluctuating water table. Previous analyses of stream waters has revealed that Fe,

93 Al, org C and limiting nutrients, such as P, were predominantly present in NNP and colloidal

4

94   fractions (Fernández-Martínez et al., 2014; Gottselig et al., 2017a; Hart et al., 1993; Hill and

95   Aplin, 2001; Jarvie et al., 2012; Martin et al., 1995). The analysis of seasonal dynamics shed

96   new light on the reasoning behind the occurrence of these elements in the colloidal fractions

97   (Dahlqvist et al., 2004; Dahlqvist et al., 2007; Pokrovsky et al., 2010). During the spring flood,

98   both the total load of transported colloids in stream water and the element concentrations

99   adhered to colloids were elevated (Pokrovsky et al., 2010). Also, seasonal changes in the flow

100   regime modify transport pathways of NNP and colloids and thereby affect the chemical

101   composition of NNP and colloids. In winter, for example, Fe serves as building block of NNP

102   and colloids in stream waters due to inflow of anoxic groundwater, whereas precipitation

103   and/or snow melt in early spring largely leach organic-rich top soil layers during flood and

104   following hydrological events, thus potentially shifting the colloidal composition to a

105   dominance of org C (Dahlqvist et al., 2004; Dahlqvist et al., 2007). In contrast, hydrological

106   pathways in late spring/early summer frequently focus on groundwater recharge than on

107   stream water inflow with exception of the afore mentioned rain events (Dahlqvist et al., 2007).

108   It seems therefore reasonable to assume that there will also be a pronounced seasonal

109   variability of NNP and colloidal bound elements.

110   Seasonal variability of dissolved and colloid-bound elements might be closely linked to

111   discharge, so that their log-log transformed concentration-discharge (C-Q) ratio can facilitate

112   the distinction between elements governed by dilution (C-Q slope ≤ -0.1), chemostatic (-0.1 <

113   slope < 0.1) or enrichment (slope ≥ 0.1) process controls (Trostle et al., 2016). This relationship

114   can moreover yield relevant information about the origin of discharge waters, how they vary

115   and thus govern particle mediated export in different catchments (e.g. Perdrial et al., 2014;

116   Trostle et al., 2016). An observed enrichment of NNP and colloids and elements occurs

117   simultaneously in conditions favoring particle adherence, particularly when organic matter is

118   present to stabilize particles (Herndon et al., 2015; Ranville and Macalady, 1997; Six et al.,

119   1999), whereas, in turn, dilutive conditions can indicate discharge waters originating from

120   inflows with lacking presence of typical NNP and colloid building blocks but with high Ca

121   and/or Si concentrations (Haygarth et al., 2004; Herndon et al., 2015; Maher, 2011).

122   In summary we note that a detailed understanding of seasonal variations of colloids vs. truly

123   dissolved (<1 nm) elements in terrestrial water catchments is still lacking. In addition, the

124   knowledge on the potential origin of the particles is limited. We hypothesize that there are

125   seasonal variations of NNP and larger colloids during the year in stream water, which differ in

126   origin depending on connectivity to the groundwater. Yet, and even though runoff generation

127   in a catchment is composed of groundwater, precipitation and stream water, the holistic

128   analysis of their NNP and colloid mass fluxes is rarely done, especially not over the course of

129   one year. To highlight the respective interactions, we monitored NNP and fine colloid fractions

130   as well as their corresponding elemental concentrations in monthly samples from several

131   components of the hydrological cycle, i.e., of rainwater, throughfall, subsurface flow, stream

132   and groundwater in accordance to hydrological monitoring of stream water discharge,

133   groundwater level and precipitation amounts. The assessment of NNP and fine colloids was

134   performed after Field Flow Fractionation (FFF), a non-destructive chromatography-like

135   technique, which can be coupled to mass spectrometry and other element-specific detectors,

136   and is routinely applied to distinguish NNP and colloids in environmental samples (Baalousha

137   et al., 2011; Nischwitz et al., 2018).

138   2. Material and methods

139   2.1 Study site

140   Samples were obtained from the Conventwald study site, which is situated in the Black Forest

141   (48°02'0 N, 7°96'0 E) near Freiburg, Germany. The site is a Level II intensive monitoring site of

142   the Pan-European International Co-operative Program on assessment and monitoring of air

143   pollution effects on forests (ICP Forests) under UN-ECE (Lang et al., 2017; Lorenz, 1995; Vries

144   et al., 2003). Two small neighboring catchments were sampled, catchment 1 with an area of

145   0.086 km² and to the east catchment 2 with an area of 0.077 km² (Sohrt, 2019). Both have an

146   average elevation of 840 m a.s.l., an average slope angle of 20°, annual mean temperatures

147   around 6.6°C, and a mean annual precipitation of 1749 mm a^{-1} (see also Lang et al. (2017) for

148   more details). The soils are Cambisols (IUSS, 2015), developed from paragneiss. Dominant tree

149   species are *Fagus sylvatica, Picea abies* and *Abies alba*. Catchment 1 is drained by a creek and

150   catchment 2 by a spring without visible surface flow.

151   Scientific instrumentation of catchment 1 was done some decades ago by the 'Forstliche

152   Versuchs- und Forschungsanstalt Baden-Württemberg', Freiburg, Germany, and consists of

153   above- and below-canopy precipitation collectors, soil moisture sensors and a discharge weir

154   at the catchment outlet. Catchment 2 was instrumented in 2013/2014 by the University of

155   Freiburg, with above- and below-canopy rainwater collectors, a weir at the catchment outlet,

156   and lateral subsurface flow samplers (10 m wide refilled trench) and with a groundwater well

157   by GFZ Potsdam.

158   2.2 Sampling

159   Monthly samples were collected from February 2015 to February 2016 from the above- and

160   below-canopy precipitation collectors (termed rainwater and throughfall), the groundwater

7

161   well, stream and spring weirs of catchments 1 and 2 as well as at the first surface visible stream

162   flow of catchment 1 ("spring"; supplementary information, Table SI1). Additionally, samples

163   integrating lateral subsurface flow from three trench depth intervals were collected

164   (collection at 10 cm depth: integration of depth 0-10 cm, 230 cm depth: 10-230 cm and

165   300 cm depth: 230-300 cm; supplementary information, Table SI1, for further details). Not all

166   samples were available at all sampling dates (supplementary information, Table SI1). Samples

167   were taken in 250 mL PE bottles. Prior to analyses, samples were stored at 4°C and analyzed

168   within two weeks. An overview of sampling dates and discharge is provided in Figure SI1

169   (supplementary information).

170   2.3 Hydrological and meteorological parameters

171   During the sampling period, meteorological data (air temperature, precipitation amounts

172   above and below the tree canopy) were recorded every 15 min and hydrological data (current

173   discharge at the weirs, soil moisture in 30 and 60 cm depth, the height of the groundwater

174   level) every 5 min (Figure 1; supplementary information, Figure SI2). The groundwater level

175   was determined via a pressure probe installed in 8.5 m below the surface. Above and below

176   tree canopy precipitation was collected via self-constructed rain collectors and amounts were

177   determined through direct scale reading.

178   In addition to the parameters recorded in the field, pH and electrical conductivity (EC) of the

179   stream water samples at catchment 2 weir as well as EC of the groundwater samples was

180   recorded in the laboratory immediately after sampling (supplementary information, Figure

181   SI2). To determine the relative contributions of groundwater vs. lateral subsurface flow into

182   the stream, concentrations of eight elements (Ca, Na, K, Mg, S, DOC, Si, Cl) were analyzed in

183   stream water, groundwater and the three depths of lateral subsurface flow collection and

184 used for end-member-mixing-analysis (EMMA; calculated according to Dietze and Dietze,

185 2013, see also Sohrt 2019). The elements were selected on the basis of recent literature (e.g.

186 Barthold et al., 2011; Frisbee et al., 2011; Guinn Garrett et al., 2012). The results and

187 robustness of the EMMA are shown in the supplementary information, Figure SI2.

188 2.4 Particle fractionation and concentration data

189 Samples were not filtered prior to analyses, in order to prevent clogging of the filter. Thus,

190 particle fractionation was directly performed via Asymmetric Flow Field Flow Fractionation

191 (AF^4, Postnova Analytics, Landsberg, Germany) coupled to a UV detector, a quadrupole

192 inductively coupled plasma-mass spectrometer with helium collision cell technology (ICP-MS;

193 Agilent 7500, Agilent Technologies, Japan) and an organic carbon detector (OCD; DOC Labor,

194 Karlsruhe, Germany). This method is particularly suitable for aqueous samples because they

195 can be analyzed in their natural state without undergoing prior processing. Fractionation

196 parameters, ICP-MS system settings and calibration as well as OCD coupling parameters and

197 calibration can be found in section 2.2 of Gottselig et al. (2017a). Total concentrations of org

198 C were assessed for the first six months of the sampling period (Feb 2015 to Jul 2015) and of

199 Al, Si, P, Ca, Mn and Fe for the second half of the sampling period (Aug 2015 to Feb 2016).

200 Colloidal org C concentrations were often below detection limit (LOD = 0.001 mmol L^{-1}).

201 NNP and fine colloids from aqueous samples were also compared to water dispersible colloids

202 (WDC), which were extracted from soil horizon aliquots of a soil pit sampling performed in

203 Nov 2013. The WDC extraction was performed and published by Missong et al. (2018a). Total

204 element concentrations of the soil horizons as well as further information on the soil pit study

205 can be found in Lang et al. (2017). WDC and total soil data were transferred to the unit μmol

206 g$_{soil}$$^{-1}$ for better comparison.

207   2.5 Data analysis

208   The ICP-MS raw data were collected in counts per second (cps) by the MassHunter

209   Workstation Software (Agilent Technologies, Japan), and OCD raw data were recorded in volt

210   detector signal (V) with the AF^4 analytical software (Postnova Analytics, Landsberg, Germany).

211   Both datasets were exported to Excel (Microsoft Corporation, Redmond, USA) for baseline

212   correction, peak integration and calculation of peak concentrations through multipoint linear

213   calibrations. In general, the particle data is referred to as 1st/2nd/3rd fraction of element X and

214   all colloidal element concentration refers to the sum of the elements concentrations in the

215   1st, 2nd and 3rd fraction. All concentration data were transferred to µmol L^{-1} for Al, Si, P, Ca, Mn

216   and Fe and to mmol L^{-1} for org C. Additionally, total elemental concentrations in the samples

217   were determined via the ICP-MS and the OCD, respectively. In contrast to the ICP-MS, which

218   also functions as a stand-alone device, the OCD measurements for total org C were realized

219   by direct injection through the AF^4 autosampler.

220   The relative proportion of particles was determined by calculating the percentage of all

221   colloidal elemental concentration of each element with respect to the total elemental

222   concentration of each element in the respective sample. The truly dissolved (<1 kDa)

223   elemental concentrations are derived as difference between the total and all colloidal

224   concentration per element.

225   For comparability reasons the concentration data measured in samples from the weirs of

226   catchment 1 and 2 over the 13 month sampling period were multiplied by discharge amount

227   at time of sampling and thus expressed as loads in the unit (µ/m)mol s^{-1}. Additionally, to

228   analyze the variability of elemental concentrations in the fractions over the sampling duration,

229   the sum of all colloidal element contents was set to 100% and the fraction concentrations

230 were then expressed in percentages of the total colloidal fraction. Predictions of colloidal

231 concentrations and stream water inflows were performed after all input data underwent $\log_{10}$

232 transformations. Pearson correlations ($p < 0.05$) were calculated using Statistica 8.0 (StatSoft

233 Europe, Hamburg, Germany).

234 2.6 Process and quality control

235 The storage capability and thus transportability of natural nanoparticles and colloids after

236 sampling is decisively determined by the stability of the particle composition and sizes as

237 collected when sampling. A first detailed assessment of the circumstances affecting colloidal

238 stability was conducted by Buffle and Leppard (1995). They recommended to keep storage

239 times as short as possible. Own unpublished work has revealed that constant refrigerated

240 storage of unprocessed stream water in pre-cleaned polyethylene or polypropylene

241 containers sustained a stability of natural colloids at least up to 14 days after sampling. Prior

242 to taking the actual sample, containers were preconditioned in triplicates with stream water

243 and the sample was taken from the center of the flowing stream without disturbance of

244 sediments. Visible fractions of leaves or further debris was not included in the sample, nor

245 was the sample processed in any way except agitation prior to injection into the AF[4].

246 The AF[4] is in theory capable of resolving the whole size spectrum between 1 and 1000 nm

247 within one fractionation run, yet the application, especially to environmental particles, has

248 proven that an optimal resolution can only be achieved when focusing on a size range with a

249 width of about 500 nm. Due to the aspired redefinition of the operationally defined dissolved

250 phase (<0.45 µm), we focused on particles between 1 and 450/500 nm. Extensive method

251 development was conducted for the AF[4] fractionation of stream water to target this particle

252 size range (Gottselig et al., 2014; Gottselig et al., 2017b). Through variation of fractionation

11

253 parameters (mainly cross flow rate and gradient), it was possible to achieve a resolution of

254 three particle fractions: 1-20 nm, >20-60 nm, >60-300 nm. Steric elution could be excluded

255 because void peaks were often lacking or negligibly small. Thus, the majority of particles in the

256 stream water samples measured to date are within the size range of 1 to 300 nm and included

257 in the <0.45 µm fraction.

258 The AF[4] fractionation is achieved despite the absence of a stationary phase. Yet, interactions

259 with the membrane defining the lower particle size cut-off cannot be neglected, especially

260 during focusing of the sample and/or at high cross flows. As reference parameter, the total

261 sample concentration per element prior to fractionation was always recorded offline by ICP-

262 MS. The comparison of total and all particulate data yielded elemental concentrations in the

263 colloidal fraction up to 99.5% of total elemental concentrations, thus allowing the conclusion

264 that no major particle loss occurs (Gottselig et al., 2017a). A detailed investigation of the AF[4]

265 recoveries of synthetic iron oxyhydroxide colloids revealed recoveries between 70 and 93%

266 (Baken et al., 2016a). These results are transferrable to natural particles given the similarity of

267 synthetic iron oxyhydroxides with natural particles.

268

269 3. Results

270 3.1 Particle fractionation

271 The fractionation of the aqueous samples with AF[4] coupled online to ICP-MS or OCD resulted

272 in three distinct particle peaks, whereby the 2nd fraction was dominated by Ca (Figure 2). Peak

273 boundaries were defined by the changing ICP-MS signal intensities between the monitored

274 elements. A similar peak pattern for aqueous samples in general was previously observed for

275 several other stream water samples in Europe (Gottselig et al., 2017a; Gottselig et al., 2017b).

276   In Gottselig et al. (2017b), samples from the Conventwald catchment were also included and

277   size measurements of the particle fractions reported. Also the particle sizes at the peak

278   boundaries were similar to those previously observed for other forest ecosystems (Gottselig

279   et al., 2017a; Gottselig et al., 2017b), reflecting a reproducible fractionation process for similar

280   sample types (section 2.6). The smallest particle size of the 1st fraction was equal to the

281   molecular weight cut-off (MWCO) of the membrane (1kDa; equivalent to r~0.66 nm, equation

282   2.2, Erickson 2009) and included particles up to approx. 20 nm hydrodynamic diameter, the

283   2nd fraction included nanoparticles between 20 and 60 nm and the 3rd fraction nanoparticles

284   >60 nm to colloids of a maximum size of approx. 300 nm (cf. Gottselig et al., 2017b; section

285   2.6). Thus, all fractionated nanoparticles and fine colloids fell within the operationally defined

286   "dissolved phase" (<0.45 µm; Marschner and Kalbitz, 2003 and references therein).

287   The findings showed that Field Flow Fractionation allows a more detailed analysis of colloid-

288   bound elements that would otherwise be assigned to the term 'dissolved', based on their size

289   being <0.45 µm. Only colloidal (1 nm to approx. 300 nm) elements were assessed, so that the

290   discrepancy to the total elemental concentration in the samples then reflected the truly

291   dissolved part. Our data showed that the portion of elements bound to colloids (here assessed

292   as the sum of the three fractions) comprised 26.8 ± 16.5% (mean ± SD) of Al, 24.3 ± 24.0% of

293   P, 22.3 ± 29.7% of Mn, and 55.0 ± 26.7% of Fe, while only 6.2 ± 10.8% of org C, 2.1 ± 7.4% of

294   Si, and 3.9 ± 4.6% of Ca was bound to or within the colloids (cf. section 2.4). The percentages

295   of org C in the colloids were thus of similar magnitude than those of Si and Ca, which was

296   lower than previously reported (Gottselig et al., 2014; Gottselig et al., 2017a) but in line with

297   previous measurements of stream water in the Conventwald (Gottselig et al., 2017b).

298   3.2 Spatial variability of nanoparticles and colloids

299   The above mentioned fractionation pattern occurred in all sample types and throughout the

300   whole sampling period (cf. Figure 2). Figure 2 displays fractograms of ICP-MS and OCD data

301   averaged for each sample type over the course of the 13 months. Raw data of ICP-MS

302   fractograms were drift corrected according to the internal standard Rh and both ICP-MS and

303   OCD data were baseline corrected prior to visualization. Between the different sample types,

304   the peak intensity varied between the fractions. The throughfall samples, for instance,

305   exhibited a dominance of particles < 20 nm occurring in the 1st fraction peak (Figure 2). In

306   contrast, the groundwater samples showed prominent signals of 20-60 nm sized particles in

307   the 2nd fraction (Figure 2), mostly dominated by the Ca signal. The peak patterns of two trench

308   samples (0-10 cm and 10-230 cm; Figure 2) closely resembled the throughfall samples (Figure

309   2). Hence, along the water transport pathway from throughfall to groundwater, NNPs were

310   partly replaced by larger particles, thus likely indicating a re-formation of the latter.

311   Apart from mere size and abundance, the elemental composition of NNP and larger colloids

312   may be indicative of their origin (Gottselig et al., 2017a). Here, the trench samples contained

313   mainly 1st fraction particles primarily consisting of org C, Al, Fe and Ca (Figure 2, Table 2). A

314   further resemblance was observed for the peak composition of all other sample types (cf.

315   Figure 2). Thus, rainwater, groundwater, trench 230-300 cm and the stream water exhibited

316   similar peak expression patterns and magnitudes (cf. Figure 2). Here, we primarily observed

317   2nd fraction particles consisting of Ca but also of P and Si and 3rd fraction particles with highest

318   average signals for org C, Si and P.

319   3.3 Yearly variation of nanoparticles and colloids

320   The colloidal concentrations of the stream water elements showed seasonal differences but

321   especially substantial concentration decreases in the months May to October after

14

322   multiplication with discharge (cf. Figure 3, left; supplementary information, Figure SI3). This

323   decline also corresponded to seasonal fluctuations in precipitation amounts and soil moisture

324   (cf. Figure 1, supplementary information, Figure SI2) and was reciprocal to the change of air

325   and stream temperature and relative contribution of groundwater in the stream as

326   determined through EMMA (cf. Figure 1; supplementary information Figure SI2).

327   The relative proportions of elements bound to a given colloid size fraction varied up to a factor

328   of ~10, for example, for 3rd fraction Ca (cf. Figure 3, supplementary information, Figure SI3)

329   over the season. Looking at P, a median range of 20.8% to 32.6% P within the 1st fraction,

330   27.1% to 39.7% P in the 2nd fraction and 29.3% to 43.4% P in the 3rd fraction relative to the

331   total colloidal loads was found (factor ~2; cf. Figure 3, supplementary information, Figure SI4).

332   The colloidal P load was lowest between April and October, yet with highest portions of P

333   found in the largest colloids during this period (cf. Figure 3, supplementary information, Figure

334   SI4). This seasonal trend was not only seen for P but also for colloidal Fe in groundwater

335   samples (supplementary information, Figure SI4). Fe in rain and stream water as well as Al and

336   Si in all sample types showed an opposing trend with an increase in 1st fraction Fe peaking

337   around May at the expense of the 3rd fraction and at steady 2nd fraction concentrations (Figure

338   3; supplementary information, Figure SI4). Further noteworthy, Ca and Mn 1st fractions

339   showed seasonal variations with peak concentrations around May at the expense of 2nd

340   fraction and at similar 3rd fraction concentrations throughout the year (Figure 3;

341   supplementary information, Figure SI4). Org C clearly dominated the 3rd fraction with the

342   exception of some spring samples (supplementary information, Figure SI4) and the occurrence

343   of 1st fraction org C in the throughfall, yet concentrations were often below detection limit

344   and thus evident seasonal patterns could not be seen.

345   3.4 Predictability of colloidal elemental composition over the course of one year

346　To better understand seasonal effects on the occurrence of elements within NNP and fine

347　colloid fractions, we correlated fraction-specific elemental and total sample concentrations in

348　accordance to our former study on European scale (Gottselig et al., 2017a). For all samples of

349　the current study, we found that the concentrations of org C, Al, P, Ca, Mn and Fe within a

350　given size fraction correlated linearly with the total element concentration (Figure 4; Table 1).

351　In contrast, no linear correlation was found for colloidal Si, thus aggravating simple occurrence

352　predictions for the element Si (Table 1).

353　The same evaluations with only the stream water samples confirmed the linear relationship

354　for the log_{10} transformed Al, P and Fe concentration, which are the elements with largest

355　proportions of colloidal phases (section 3.1). In contrast, respective relationships for org C, Si,

356　Ca and Mn were rather scattered (Table 1, bottom). For org C this lacking relationship for the

357　stream water samples can most likely be attributed to the few data points available, whereas

358　for Ca the relationship found for all sample types was clearly absent when only considering

359　the stream water (cf. Table 1) because the precipitation data (rainwater and throughfall)

360　created the linearity (cf. Figure 5). Concerning P, the linear relationship was confirmed by the

361　stream water data and here also showed significant linear correlations for the 3rd fraction to

362　total P relationship.

363　3.5 Stream water composition

364　A comparison between sample types for the afore mentioned relationships can reflect

365　similarities in colloidal origin and thus allow to identify potential inflows into the stream.

366　Taking into consideration that larger sized colloids were detected in the rainwater after it

367　passed through the canopy (rainwater in comparison to throughfall), we investigated the

368　change in colloid elemental concentration in the aqueous samples and in comparison to WDC

369 extracted from the different soil horizons. As shown in Figure 5 for all elements, the chemical

370 composition of stream and groundwater (and rainwater for Al and Fe) was similar.

371 The concentration bi-plots (Figure 5) also revealed that different sample types were

372 characterized by different element loads, e.g. for Al, Mn and Fe, ground and stream water

373 were found in the lowest concentration range of both total and colloidal element

374 concentrations. Throughfall and rainwater samples clearly exhibited lowest concentrations in

375 total Si and Ca, but not necessarily lower colloidal concentrations of these elements,

376 respectively. In contrast, the trench samples clustered at elevated colloidal and total element

377 loads of Al, P, Fe, and Mn. However, the chemical composition of WDC was not reflected by

378 any aqueous sample (Figure 5). Thus, the WDC method potentially overestimates the actual

379 element mobilization from soil profiles (Missong et al., 2018b).

380 The C-Q relationships revealed seven significant correlations (Pearson, $p<0.05$) out of which

381 six were from 3rd fraction elemental concentrations. The only significant correlation of 2nd

382 fraction concentrations with discharge was for P in catchment 1 weir at a slope of 0.57 with

383 $r^2=0.38$. Further, for the 3rd fraction, org C showed significant correlations for catchment 1

384 spring (slope = -0.36, r^2 = 0.47) and weir (slope = -0.63, r^2 = 0.55) samples, Al for catchment 1

385 (slope = 0.55, r^2 = 0.60) and catchment 2 (slope = 0.51, r^2 = 0.67) weirs and Fe also for

386 catchment 1 (slope = 0.34, r^2 = 0.45) and catchment 2 (slope = 0.54, r^2 = 0.67) weirs.

387 Apparently, org C, Al and Fe guided the overall role of colloidal fluxes for the total element

388 loss from the ecosystem.

389 3.6 Interdependency of elemental concentrations

390 There is a high probability to encounter multi-element particles in natural samples. Thus,

391 Pearson correlations were calculated for all sample types to assess the co-transport of

392   different elements within one fraction and thus to infer that these elements occurred within

393   one particle in the fraction. Table 2 provides an overview over all significant (p<0.05) Pearson

394   correlation coefficients between elements of the respective fraction and sample type. All

395   sample types, excluding the trench, showed a low number of significant correlations. In

396   groundwater and rainwater samples, mainly correlations between Ca and Si as well as Fe and

397   Al were found; in the throughfall samples additionally org C particles associated to Al, P and/or

398   Fe occurred (cf. Table 2). The correlations of the trench samples included all trench depths

399   due to low sample numbers of especially the deepest trench collection (n=3; cf.

400   supplementary information, Table SI1). Here, especially for the 1st fraction many potential

401   particle compositions were detected with decreasing numbers as particle sizes increased (cf.

402   Table 2). Stream water results showed highest similarity to groundwater and rainwater

403   correlations (cf. Table 2).

404

405   4. Discussion

406   4.1 Relevance of natural nanoparticles and colloids in forest ecosystem compartments

407   The percentage of elements within the NNP and colloid fractions in relation to the total

408   elemental concentrations was used as a straightforward calculation to determine the

409   relevance of NNP and colloids in stream water. For the current study, the percentage of

410   elemental binding to NNP and colloids was substantial for Al, P, Mn and especially Fe with

411   average percentages between 22 and 55% (cf. section 3.1), thus confirming their steady

412   occurrence also in colloidal form despite the low overall particle concentrations in the stream

413   water (cf. supplementary information, Figure SI5). Yet, with the exception of Fe, Mn and Si,

414   the percentages were markedly lower than found for other stream waters (Dahlqvist et al.,

415 2004; Gottselig et al., 2017a; Hill and Aplin, 2001; Jarvie et al., 2012; Martin et al., 1995; Wen

416 et al., 1999). Hill and Aplin (2001) and Jarvie et al. (2012), for instance, found average Al

417 binding in riverine samples between 45 and 55%, thus exceeding our proportions by a factor

418 of two. Also, studies on P in NNP and colloid fractions frequently reported binding percentages

419 between 45 and 66% (Gottselig et al., 2017a; Jarvie et al., 2012; Missong et al., 2018b) in

420 relation to 24% found here. The largest difference to other ecosystems was found for C, where

421 we determined that NNP and colloids contributed to 6% of org C in solution, while other

422 studies found binding percentages between 20 and 60% org C (Gottselig et al., 2017a; Jarvie

423 et al., 2012; Martin et al., 1995; Wen et al., 1999). Nevertheless, the data agree with

424 assessments on similar Conventwald stream samples (Gottselig et al., 2017b). Hence, we

425 suggest that the lower proportion of elements bound to NNP and colloids relative to other

426 studies reflects the specific flow pathways of this forest ecosystem, where a steep slope allows

427 the generation of stream water without further seepage inputs from soil solutions.

428 Noteworthy, the elements detected in the NNP and fine colloid fractions occurred in three

429 distinct size ranges (Gottselig et al., 2017a; Figure 2; see also Jiang et al., 2015; Missong et al.,

430 2016), and not solely as particles <25 nm as reported by Dahlqvist et al. (2004) and Andersson

431 et al. (2006). The contribution of these fractions to total element loads varied but were, at

432 least in part, also specific for a given sample compartment. Throughfall and soil leachates

433 integrating from 0 to 2.3 m of soil showed a dominance of the 1st fraction peak, i.e., of particles

434 <20 nm. Rainwater, deep trench samples and stream water showed the occurrence of all

435 peaks (Figure 2), but with different P/Ca ratio in comparison to the groundwater samples. This

436 finding indicates different mixing processes in the ecosystem. Throughfall, which also received

437 additional org C from the canopy (Figure 2), likely infiltrated the soil rapidly and maintained

438 its NNP and fine colloidal signature down to 2.3 m depth. Soil leachate from >2.3 m depth

439 showed some groundwater contribution. Rainwater may have influenced the stream's

440 chemical composition, but due to the low areal extension of the streams a dominating impact

441 seems unlikely. The rainwater input largely showed similarities to groundwater, which likely

442 feeds the stream.

443 Not all findings can be explained by mixing processes. The lacking dominance of the small NNP

444 <20 nm in the groundwater as compared with throughfall, for instance, suggests that also

445 during water partitioning in the ecosystem NNP and larger colloids are dynamic. Particularly

446 the larger, Ca-rich particles in the size range of 20-60 nm must have reformed in the ecosystem

447 and cannot merely stem from leaching inputs. The underlying kinetics of NNP breakdown and

448 re-aggregation remain poorly constraint; yet, they must occur at annual scale to justify the

449 seasonal patterns.

450 4.2 Seasonal patterns

451 Microclimate is usually considered as one main driver of the seasonality in element fluxes (e.g.

452 Foster and Bhatti, 2006). Elemental loads in catchment 1 and 2 weirs fluctuated reciprocal to

453 air and thus stream water temperature and stream water electrical conductivity but parallel

454 to soil moisture and precipitation (Figure 1 and 3; supplementary information, Figure SI1).

455 These fluctuations were most pronounced between summer and winter. Indeed, total

456 colloidal elemental concentrations were substantially lower in summer than in winter. This

457 trend was also observed in other ecosystems, e.g., for Ca in particles <0.22 μm in an arctic

458 river where the respective concentrations declined almost 4-fold from winter to summer

459 loads, with substantial dilution occurring due to the spring flood (cf. Dahlqvist et al., 2004). In

460 our study, no distinct spring flood event occurred from multiple rainfall or snowmelt events

461 (supplementary information, Figure SI2), yet, due to lower discharge and thus water amounts

462 in the ecosystem in summer months, the colloidal elemental loads decreased accordingly (e.g.

463 Figure 3).

464 Intriguingly, different elements responded differently to this seasonal trend. For example, the

465 colloidal P concentrations showed a maximum in February and March in both stream and

466 groundwater, whereas colloidal Ca concentrations increased after July (supplementary

467 information, Figure SI5). These differences reflect the different sources of the elements. While

468 P is hardly leached (Bol et al., 2016) and thus likely stemmed from surface runoff (Heathwaite

469 and Dils, 2000), the occurrence of a deep layer rich in easily exchangeable Ca (Uhlig and von

470 Blanckenburg, 2019) fed groundwater and explained the elevated P/Ca ratios therein (Figure

471 2). Hence, the dynamics of colloidal P differed from the groundwater coupled dynamics of Ca.

472 Existing or lacking correlations on the variability between the binding percentages of the

473 different NNP and colloid fractions provide insight into seasonal changes between the particle

474 fractions (Figure 3; supplementary information, Figure SI3 and SI4). In this regard, the

475 dynamics of Fe and Al as well as of org C and P were closely coupled while that of other

476 elements were not (Table 2), also reflecting their different contribution to overall colloid loads.

477 Through an assessment of fraction concentrations of multiple German streams including the

478 Conventwald, Gottselig et al. (2017b) determined building block elements of 1st fraction NNP

479 to be metals or org C, while 2nd fraction NNP identified as Fe-org C or metal particles and 3rd

480 fraction NNP and colloids largely were found to be clay minerals and/or larger Fe-org C

481 compounds. Fe as micronutrient and fundamental constituent of all three fractions shows a

482 clear seasonality within the 1st fraction (<20 nm NNP) with minimal occurrence in stream

483 waters in November and maxima in March and June (Figure 3). These trends may be

484 interpreted in terms of a nutrient depletion in November following the growth and

485   development period of the plants, and an enrichment when biogeochemical weathering rates

486   are high towards end of spring (Yesavage et al., 2012). Moreover, the occurrence of Fe in the

487   1st fraction seems to have a reciprocal effect on the 3rd fraction, suggesting that different

488   colloidal sizes are linked via input and aggregation processes, for instance.

489   Org C often correlates well with Fe in micrometer sized particles (e.g. Gandois et al., 2010;

490   Gottselig et al., 2017b) and can be indicative of soil runoff (McIntosh et al., 2017). Yet, org C

491   showed lower concentrations in Conventwald stream water (supplementary information,

492   Figure SI3 and SI4) in comparison to earlier findings (Gottselig et al., 2017b; Jarvie et al., 2012;

493   Martin et al., 1995; Wen et al., 1999). Single higher concentrations were detected in

494   throughfall in May (0.4 mmol L^{-1}) and in soil leachate samples of September and October (0-

495   10 cm, 0.6 and 0.7 mmol L^{-1}; data not shown). However, these finding apparently do not

496   influence org C concentrations in stream water particles. Thus, no seasonality of org C was

497   found. The same was true for the major components of clay minerals (Al and Si), a typical

498   component of 3rd fraction stream water particles.

499   A further element generally not in focus in the context of P in slightly acidic forest catchments

500   but which showed high concentrations in all three stream water particle fractions and high

501   binding percentages in the 2nd fraction was Ca (Figure 1 and 3). As previously discussed by

502   Missong et al. (2018b), Ca seems to be a further important building block structure, especially

503   in the context of P, and potentially even independent of pH. Despite a siliceous bedrock, a

504   constant layer rich in exchangeable Ca which is also hydrologically connected to the stream

505   must be present due to the high concentrations in stream and groundwater as well as trench

506   samples (cf. Figure 5), as well as the constant binding percentages in all three fractions with

507   only slight effect of seasonality (Figure 3). In fact, this layer was found in the deep subsoil

508   beneath ~3 m depth (Uhlig and von Blanckenburg, 2019). Hence, even if surface soils are

509   acidified, it may be essential to include Ca in the analysis of building block structures of NNP

510   and fine colloids in acidic forest ecosystems.

511   4.3 Stream water inflows and further influential parameters

512   The origin of particles in stream waters can be traced through assessment of a combination

513   of hydrological dynamics, elemental reaction to changes in discharge as well as indicator

514   elements of different flow pathways. Pokrovsky et al. (2010) distinguished their data according

515   to dynamics based on two inflows into stream water: i) groundwater poor in organic matter

516   but high in truly dissolved species released from the bedrock, and ii) shallow soil waters rich

517   in organics and thus NNP and colloids. Figure 5 indicates that the majority of water entering

518   the stream must be derived from groundwater and showed additional occasional similarities

519   to subsoil (>2.3 m) trench collection, which were most probably also mainly influenced by

520   groundwater. Following the classification introduced by Pokrovsky et al. (2010), these findings

521   imply that the influence of shallow soil water was minimal in stream waters of the

522   Conventwald due to the juxtaposition of stream and groundwater to data from the upper

523   trench collection (<2.3 m) and soil pits (Figure 5; Lang et al., 2017; Missong et al., 2018a).

524   A further observation from the plots of Figure 5 is the gradual variation from aqueous sample

525   concentrations to the data from the soil pits. Particularly for Fe and Al, but also for org C, P

526   and Mn, the NNP and fine colloid concentrations seem to represent a sub-fraction of the

527   concentrations derived for WDC (Missong et al., 2018a). In contrast, Ca shows enrichment in

528   NNP and fine colloids at similar total Ca concentrations (Figure 5). In no case the

529   concentrations of WDC were reached in aqueous colloids, suggesting that the former may only

530   indicate nutrient mobilization far off from realistic colloidal concentration ranges detected in

531   the latter.

532 The C-Q relationships revealed that an increase in discharge has a significant enrichment effect

533 only for P in 2nd fraction particles and Al and Fe in 3rd fraction particles, whereas, in contrast,

534 org C concentrations decline with increasing discharge (cf. section 3.4). This finding was

535 indicative of a dominant non-surface water source entering the stream at high discharge, due

536 to the dilutive C-Q behavior for org C, which was additionally rich in Ca and Si (Figure 5).

537

538 5. Conclusions

539 The assessment of natural nanoparticles and colloids in multiple aqueous compartments of a

540 forest ecosystem over the course of one year by means of Field Flow Fractionation has

541 revealed that these natural particles occur throughout the year in the analyzed water

542 compartments. Judging from the fractograms, rainwater, stream water and groundwater

543 contained similar particle distributions and throughfall and soil leachates. Nevertheless, the

544 elemental loads varied with higher values in winter than in summer. Intriguingly, this variation

545 only affected one size class per element and sample while at least one of the three fractions

546 (per element) was fairly stable throughout the whole year. The seasonal occurrence of NNP

547 and colloids is thus not only affected by seasonal variations in water fluxes but also by seasonal

548 dynamics in particle reformation by dispersion, aggregation, and mixing with different

549 elements.

550 Different elements bound to NNP and colloids partly originated from different sources. While

551 P mainly stemmed from processes at the terrestrial land surface, the origin of Ca was clearly

552 related to interactions in the groundwater aquifer. As a result, the seasonal dynamics of these

553 different colloidal element loads were not immediately coupled and resulted, thus, in different

554 element ratios of, e.g., P/Ca in throughfall and soil leachates compared to ground- and stream

555 water, respectively.

556

557

558 *Acknowledgements*

References

564 Andersson, K., Dahlqvist, R., Turner, D., Stolpe, B., Larsson, T., Ingri, J., Andersson, P., 2006. Colloidal
565   rare earth elements in a boreal river: Changing sources and distributions during the spring flood.
566   Geochim. Cosmochim. Acta 70, 3261–3274. https://doi.org/10.1016/j.gca.2006.04.021.

567 Baalousha, M., Stolpe, B., Lead, J.R., 2011. Flow field-flow fractionation for the analysis and
568   characterization of natural colloids and manufactured nanoparticles in environmental systems: A
569   critical review. J. Chroma. A 1218, 4078–4103. https://doi.org/10.1016/j.chroma.2011.04.063.

570 Baik, M.-H., Yun, J.-I., Bouby, M., Hahn, P.-S., Kim, J.-I., 2007. Characterization of aquatic groundwater
571   colloids by a laser-induced breakdown detection and ICP-MS combined with an asymmetric flow
572   field-flow fractionation. Korean J. Chem. Eng. 24, 723–729. https://doi.org/10.1007/s11814-007-
573   0033-7.

574 Baken, S., Moens, C., van der Grift, B., Smolders, E., 2016a. Phosphate binding by natural iron-rich
575   colloids in streams. Water Res. 98, 326–333. https://doi.org/10.1016/j.watres.2016.04.032.

576 Baken, S., Regelink, I.C., Comans, R.N.J., Smolders, E., Koopmans, G.F., 2016b. Iron-rich colloids as
577   carriers of phosphorus in streams: A field-flow fractionation study. Water Res. 99, 83–90.
578   https://doi.org/10.1016/j.watres.2016.04.060.

579 Barthold, F.K., Tyralla, C., Schneider, K., Vaché, K.B., Frede, H.-G., Breuer, L., 2011. How many tracers
580   do we need for end member mixing analysis (EMMA)? A sensitivity analysis. Water Resour. Res.
581   47. https://doi.org/10.1029/2011WR010604.

582 Bol, R., Julich, D., Brödlin, D., Siemens, J., Kaiser, K., Dippold, M.A., Spielvogel, S., Zilla, T., Mewes, D.,
583   Blanckenburg, F. von, Puhlmann, H., Holzmann, S., Weiler, M., Amelung, W., Lang, F., Kuzyakov, Y.,
584   Feger, K.-H., Gottselig, N., Klumpp, E., Missong, A., Winkelmann, C., Uhlig, D., Sohrt, J., Wilpert,
585   K.v., Wu, B., Hagedorn, F., 2016. Dissolved and colloidal phosphorus fluxes in forest ecosystems—
586   an almost blind spot in ecosystem research. J. Plant Nutr. Soil Sci. 179, 425–438.
587   https://doi.org/10.1002/jpln.201600079.

588 Buffle, J., Leppard, G.G., 1995. Characterization of aquatic colloids and macromolecules. 2. Key role of
589   physical structures on analytical results. Environ. Sci. Technol. 29, 2176–2184.
590   https://doi.org/10.1021/es00009a005.

591 Cizdziel, J.V., Guo, C., Steinberg, S.M., Yu, Z., Johannesson, K.H., 2008. Chemical and colloidal analyses
592   of natural seep water collected from the exploratory studies facility inside Yucca Mountain,
593   Nevada, USA. Environ. Geochem. Health 30, 31–44. https://doi.org/10.1007/s10653-007-9105-1.

594 Dahlqvist, R., Andersson, K., Ingri, J., Larsson, T., Stolpe, B., Turner, D., 2007. Temporal variations of
595   colloidal carrier phases and associated trace elements in a boreal river. Geochim. Cosmochim. Acta
596   71, 5339–5354. https://doi.org/10.1016/j.gca.2007.09.016.

597 Dahlqvist, R., Benedetti, M.F., Andersson, K., Turner, D., Larsson, T., Stolpe, B., Ingri, J., 2004.
598   Association of calcium with colloidal particles and speciation of calcium in the Kalix and Amazon
599   rivers. Geochim. Cosmochim. Acta 68, 4059–4075. https://doi.org/10.1016/j.gca.2004.04.007.

600 Degueldre, C., Triay, I., Kim, J.-I., Vilks, P., Laaksoharju, M., Miekeley, N., 2000. Groundwater colloid
601   properties: A global approach. Appl. Geochem. 15, 1043–1051. https://doi.org/10.1016/S0883-
602   2927(99)00102-X.

603 Dietze, M., Dietze, E., 2013. EMMAgeo: End-member modelling algorithm and supporting functions for
604   grain-size analysis. R package version 0.9 1.

605 Erickson, H.P., 2009. Size and shape of protein molecules at the nanometer level determined by
606   sedimentation, gel filtration, and electron microscopy. Biol. Proced. Online 11, 32–51.
607   https://doi.org/10.1007/s12575-009-9008-x.

608 Fernández-Martínez, M., Vicca, S., Janssens, I.A., Sardans, J., Luyssaert, S., Campioli, M., Chapin Iii, F.S.,
609   Ciais, P., Malhi, Y., Obersteiner, M., Papale, D., Piao, S.L., Reichstein, M., Roda, F., Penuelas, J.,
610   2014. Nutrient availability as the key regulator of global forest carbon balance. Nat. Clim. Chang.
611   4, 471–476. https://doi.org/10.1038/nclimate2177.

612 Foster, N.W., Bhatti, J.S., 2006. Forest ecosystems: Nutrient cycling. Encyclopedia of soil science. New
613   York: Taylor & Francis Group, 718–721.

614 Frisbee, M.D., Phillips, F.M., Campbell, A.R., Liu, F., Sanchez, S.A., 2011. Streamflow generation in a
615   large, alpine watershed in the southern Rocky Mountains of Colorado: Is streamflow generation
616   simply the aggregation of hillslope runoff responses? Water Resour. Res. 47.
617   https://doi.org/10.1029/2010WR009391.

618 Gandois, L., Tipping, E., Dumat, C., Probst, A., 2010. Canopy influence on trace metal atmospheric
619   inputs on forest ecosystems: Speciation in throughfall. Atmos. Environ. 44, 824–833.
620   https://doi.org/10.1016/j.atmosenv.2009.11.028.

621 Gottselig, N., Amelung, W., Kirchner, J.W., Bol, R., Eugster, W., Granger, S.J., Hernández-Crespo, C.,
622   Herrmann, F., Keizer, J.J., Korkiakoski, M., Laudon, H., Lehner, I., Loefgren, S., Lohila, A., Macleod,
623   C.J.A., Moelder, M., Mueller, C., Nasta, P., Nischwitz, V., Paul-Limoges, E., Pierret, M.-C., Pilegaard,
624   K., Romano, N., Sebastià, M.-T., Staehli, M., Voltz, M., Vereecken, H., Siemens, J., Klumpp, E.,
625   2017a. Elemental composition of natural nanoparticles and fine colloids in European forest stream
626   waters and their role as phosphorus carriers. Global Biogeochem. Cycles 31, 1592–1607.
627   https://doi.org/10.1002/2017GB005657.

628 Gottselig, N., Bol, R., Nischwitz, V., Vereecken, H., Amelung, W., Klumpp, E., 2014. Distribution of
629   phosphorus-containing fine colloids and nanoparticles in stream water of a forest catchment.
630   Vadose Zone J. 13. https://doi.org/10.2136/vzj2014.01.0005.

631 Gottselig, N., Nischwitz, V., Meyn, T., Amelung, W., Bol, R., Halle, C., Vereecken, H., Siemens, J.,
632   Klumpp, E., 2017b. Phosphorus binding to nanoparticles and colloids in forest stream waters.
633   Vadose Zone J. 16. https://doi.org/10.2136/vzj2016.07.0064.

634 Guinn Garrett, C., Vulava, V.M., Callahan, T.J., Jones, M.L., 2012. Groundwater–surface water
635   interactions in a lowland watershed: Source contribution to stream flow. Hydrol. Process. 26,
636   3195–3206. https://doi.org/10.1002/hyp.8257.

637 Hart, B.T., Douglas, G.B., Beckett, R., Vanput, A., Vangrieken, R.E., 1993. Characterization of colloidal
638   and particulate matter transported by the Magela Creek system, Northern Australia. Hydrol.
639   Process. 7, 105–118. https://doi.org/10.1002/hyp.3360070111.

640 Hartland, A., Lead, J.R., Slaveykova, V., O'Carroll, D., Valsami-Jones, E., 2013. The Environmental
641   Significance of Natural Nanoparticles. Nature Education Knowledge 4.

642 Haygarth, P., Turner, B.L., Fraser, A., Jarvis, S., Harrod, T., Nash, D., Halliwell, D., Page, T., Beven, K.,
643   2004. Temporal variability in phosphorus transfers: Classifying concentration? discharge event
644   dynamics. Hydrol. Earth Sys. Sci. Disc. 8, 88–97. https://hal.archives-ouvertes.fr/hal-00304795.

645 Haygarth, P.M., Warwick, M.S., House, W.A., 1997. Size distribution of colloidal molybdate reactive
646   phosphorus in river waters and soil solution. Water Res. 31, 439–448.
647   https://doi.org/10.1016/S0043-1354(96)00270-9.

648 Heathwaite, A.L., Dils, R.M., 2000. Characterising phosphorus loss in surface and subsurface
649   hydrological pathways. Sci. Total Environ. 251, 523–538. https://doi.org/10.1016/s0048-
650   9697(00)00393-4.

651 Herndon, E.M., Dere, A.L., Sullivan, P.L., Norris, D., Reynolds, B., Brantley, S.L., 2015. Landscape
652   heterogeneity drives contrasting concentration–discharge relationships in shale headwater
653   catchments. Hydrol. Earth Syst. Sci. 19, 3333–3347. https://doi.org/10.5194/hess-19-3333-2015.

654 Hill, D.M., Aplin, A.C., 2001. Role of colloids and fine particles in the transport of metals in rivers
655   draining carbonate and silicate terrains. Limnol. Oceanogr. 46, 331–344.
656   https://doi.org/10.4319/lo.2001.46.2.0331.

657 IUSS, 2015. World reference base for soil resources 2014, update 2015. International soil classification
658   system for naming soils and creating legends for soil maps. World Soil Resources Reports 106.

659 Jarvie, H.P., Neal, C., Rowland, A.P., Neal, M., Morris, P.N., Lead, J.R., Lawlor, A.J., Woods, C., Vincent,
660   C., Guyatt, H., Hockenhull, K., 2012. Role of riverine colloids in macronutrient and metal
661   partitioning and transport, along an upland-lowland land-use continuum, under low-flow
662   conditions. Sci. Total Environ. 434, 171–185. https://doi.org/10.1016/j.scitotenv.2011.11.061.

663 Jiang, X., Bol, R., Nischwitz, V., Siebers, N., Willbold, S., Vereecken, H., Amelung, W., Klumpp, E., 2015.
664   Phosphorus Containing Water Dispersible Nanoparticles in Arable Soil. J. Environ. Qual. 44, 1772–
665   1781. https://doi.org/10.2134/jeq2015.02.0085.

666 Lang, F., Krüger, J., Amelung, W., Willbold, S., Frossard, E., Bünemann, E.K., Bauhus, J., Nitschke, R.,
667   Kandeler, E., Marhan, S., 2017. Soil phosphorus supply controls P nutrition strategies of beech
668   forest ecosystems in Central Europe. Biogeochem. 136, 5–29. https://doi.org/10.1007/s10533-
669   017-0375-0.

670 Lorenz, M., 1995. International co-operative programme on assessment and monitoring of air pollution
671   effects on forests-ICP forests. Water Air Soil Pollut. 85, 1221–1226.
672   https://doi.org/10.1007/BF00477148.

673 Maher, K., 2011. The role of fluid residence time and topographic scales in determining chemical fluxes
674   from landscapes. Earth Planet. Sci. Lett. 312, 48–58. https://doi.org/10.1016/j.epsl.2011.09.040.

675 Marschner, B., Kalbitz, K., 2003. Controls of bioavailability and biodegradability of dissolved organic
676   matter in soils. Geoderma 113, 211–235. https://doi.org/10.1016/s0016-7061(02)00362-2.

677 Martin, J.M., Dai, M.H., Cauwet, G., 1995. Significance of colloids in the biogeochemical cycling of
678   organic-carbon and trace-metals in the Venice lagoon (Italy). Limnol. Oceanogr. 40, 119–131.
679   https://doi.org/10.4319/lo.1995.40.1.0119.

680 McIntosh, J.C., Schaumberg, C., Perdrial, J., Harpold, A., Vázquez-Ortega, A., Rasmussen, C., Vinson, D.,
681   Zapata-Rios, X., Brooks, P.D., Meixner, T., 2017. Geochemical evolution of the Critical Zone across
682   variable time scales informs concentration-discharge relationships: Jemez River Basin Critical Zone
683   Observatory. Water Resour. Res. 53, 4169–4196. https://doi.org/10.1002/2016WR019712.

684 Missong, A., Bol, R., Nischwitz, V., Krüger, J., Lang, F., Siemens, J., Klumpp, E., 2018a. Phosphorus in
685   water dispersible-colloids of forest soil profiles. Plant Soil 427, 71–86.
686   https://doi.org/10.1007/s11104-017-3430-7.

687 Missong, A., Bol, R., Willbold, S., Siemens, J., Klumpp, E., 2016. Phosphorus forms in forest soil colloids
688   as revealed by liquid-state 31P-NMR. J. Plant Nutr. Soil Sci. 179, 159–167.
689   https://doi.org/10.1002/jpln.201500119.

690 Missong, A., Holzmann, S., Bol, R., Nischwitz, V., Puhlmann, H., Wilpert, K.v., Siemens, J., Klumpp, E.,
691   2018b. Leaching of natural colloids from forest topsoils and their relevance for phosphorus
692   mobility. Sci. Total Environ. 634, 305–315. https://doi.org/10.1016/j.scitotenv.2018.03.265.

693 Neubauer, E., Köhler, S.J., Kammer, F. von der, Laudon, H., Hofmann, T., 2013. Effect of pH and Stream
694   Order on Iron and Arsenic Speciation in Boreal Catchments. Environ. Sci. Technol. 47, 7120–7128.
695   https://doi.org/10.1021/es401193j.

696 Nischwitz, V., Gottselig, N., Missong, A., Klumpp, E., Braun, M., 2018. Extending the capabilities of field
697   flow fractionation online with ICP-MS for the determination of particulate carbon in latex and
698   charcoal. J. Anal. Atomic Spectr. 33, 1363–1371. https://doi.org/10.1039/C8JA00101D.

699 Perdrial, J.N., McIntosh, J., Harpold, A., Brooks, P.D., Zapata-Rios, X., Ray, J., Meixner, T., Kanduc, T.,
700   Litvak, M., Troch, P.A., 2014. Stream water carbon controls in seasonally snow-covered mountain
701   catchments: Impact of inter-annual variability of water fluxes, catchment aspect and seasonal
702   processes. Biogeochem. 118, 273–290. https://doi.org/10.1007/s10533-013-9929-y.

703 Perry, D.A., Oren, R., Hart, S.C. 14.4 Chemical Properties of Soils. In: Forest ecosystems: JHU Press;
704   2008. p. 269–281.

705 Pokrovsky, O.S., Viers, J., Shirokova, L.S., Shevchenko, V.P., Filipov, A.S., Dupré, B., 2010. Dissolved,
706   suspended, and colloidal fluxes of organic carbon, major and trace elements in the Severnaya Dvina
707   River and its tributary. Chem. Geol. 273, 136–149.
708   https://doi.org/10.1016/j.chemgeo.2010.02.018.

709 Ranville, J.F., Macalady, D.L. Natural organic matter in catchments. In: Saether OM, Caritat P de,
710   editors. Geochemical processes, weathering and groundwater recharge in catchments; 1997. p.
711   263–303.

712 Regelink, I.C., Koopmans, G.F., van der Salm, C., Weng, L., van Riemsdijk, W.H., 2013. Characterization
713   of Colloidal Phosphorus Species in Drainage Waters from a Clay Soil Using Asymmetric Flow Field-
714   Flow Fractionation. J. Environ. Qual. 42, 464–473. https://doi.org/10.2134/jeq2012.0322.

715 Regelink, I.C., Voegelin, A., Weng, L.P., Koopmans, G.F., Comans, R.N.J., 2014. Characterization of
716   Colloidal Fe from Soils Using Field-Flow Fractionation and Fe K-Edge X-ray Absorption
717   Spectroscopy. Environ. Sci. Technol. 48, 4307–4316. https://doi.org/10.1021/es405330x.

718 Rosenthal, E., 1987. Chemical composition of rainfall and groundwater in recharge areas of the Bet
719   Shean-Harod multiple aquifer system, Israel. J. Hydrol. 89, 329–352. https://doi.org/10.1016/0022-
720   1694(87)90185-5.

721 Saito, T., Hamamoto, T., Mizuno, T., Iwatsuki, T., Tanaka, S., 2015. Comparative study of granitic and
722   sedimentary groundwater colloids by flow-field flow fractionation coupled with ICP-MS. J. Anal.
723   Atomic Spectr. 30, 1229–1236. https://doi.org/10.1039/C5JA00088B.

724 Six, J., Elliott, E.T., Paustian, K., 1999. Aggregate and soil organic matter dynamics under conventional
725   and no-tillage systems. Soil Sci. Soc. Am. J. 63, 1350–1358.
726   https://doi.org/10.2136/sssaj1999.6351350x.

727 Sohrt J., 2019. Cycling of Phosphorus in Temperate Forested Hillslopes. Dissertation, Albert-Ludwigs-
728   Universität Freiburg.

729 Trostle, K.D., Ray Runyon, J., Pohlmann, M.A., Redfield, S.E., Pelletier, J., McIntosh, J., Chorover, J.,
730   2016. Colloids and organic matter complexation control trace metal concentration-discharge
731   relationships in Marshall Gulch stream waters. Water Resour. Res. 52, 7931–7944.
732   https://doi.org/10.1002/2016WR019072.

733 Uhlig, D., von Blanckenburg, F., 2019. How slow rock weathering balances nutrient loss during fast
734   forest floor turnover in montane, temperate forest ecosystems. Front. Earth Sci. 7, 159.
735   https://doi.org/10.3389/feart.2019.00159.

736 Vries, W. de, Reinds, G.J., Vel, E., 2003. Intensive monitoring of forest ecosystems in Europe: 2:
737   Atmospheric deposition and its impacts on soil solution chemistry. For. Ecol. Manage. 174, 97–115.
738   https://doi.org/10.1016/S0378-1127(02)00030-0.

739 Wen, L.S., Santschi, P., Gill, G., Paternostro, C., 1999. Estuarine trace metal distributions in Galveston
740   Bay: importance of colloidal forms in the speciation of the dissolved phase. Mar. Chem. 63, 185–
741   212. https://doi.org/10.1016/s0304-4203(98)00062-0.

742 Yesavage, T., Fantle, M.S., Vervoort, J., Mathur, R., Jin, L., Liermann, L.J., Brantley, S.L., 2012. Fe cycling
743   in the Shale Hills Critical Zone Observatory, Pennsylvania: An analysis of biogeochemical
744   weathering and Fe isotope fractionation. Geochim. Cosmochim. Acta 99, 18–38.
745   https://doi.org/10.1016/j.gca.2012.09.029.

746

Table 1: Top: Relations of fraction to total concentrations across all samples taken. Si: Fraction-specific median and percentage of fraction specific Si relative to all colloidal Si; org C, Al, P, Mn, Fe: Fraction-specific as function of total sample concentrations, linear regression slope (m) and intercepts (b) of $\log_{10}$ transformed data. n = 47; bottom: Relations of fraction to total concentrations across all stream water samples taken. Si, org C, Ca, Mn: Fraction-specific median and percentage of fraction specific relative to all colloidal concentrations; Al, P, Fe: Fraction-specific as function of total sample concentrations, linear regression slope (m) and intercepts (b) of $\log_{10}$ transformed data. n = 21; unit: µmol/L, org C: mmol/L; asterix: significant linear correlations (Pearson correlation, $p<0.05$). If elements are marked with * all data in the corresponding columns is significantly correlated, otherwise m and b are marked.

all aqueous samples

fraction	Si median	%all part.	org C m	org C b	Al* m	Al* b	P* m	P* b	Ca* m	Ca* b	Mn* m	Mn* b	Fe* m	Fe* b
1st	0.06	30.4	0.40	-1.80	0.75	-1.33	0.35	-1.53	0.33	-0.75	0.46	-2.22	0.63	-1.32
2nd	0.07	35.8	2.43	-1.14	0.78	-1.65	0.28	-1.62	0.42	-0.60	0.18	-2.31	0.41	-1.63
3rd	0.04	33.8	1.72*	-1.58*	0.46	-1.58	0.24	-1.44	0.62	-1.97	0.13	-3.06	0.21	-1.80
all	0.11		2.40*	-0.82*	0.70	-0.91	0.30	-1.02	0.42	-0.40	0.26	-1.92	0.49	-0.94

stream water samples

fraction	Si median	%all part.	org C median	%all part.	Ca median	%all part.	Mn median	%all part.	Al m	Al b	P m	P b	Fe m	Fe b
1st	0.08	31.4	0.005	23.8	0.68	27.1	0.0004	17.7	0.28	-1.57	0.32*	-1.62*	0.08	-2.20
2nd	0.06	35.9			1.57	63.5	0.0016	69.4	1.06	-1.35	0.52	-1.65	-0.01	-2.31
3rd	0.04	32.8	0.002	76.2	0.25	9.9	0.0004	15.7	0.86*	-1.24*	0.29*	-1.55*	0.72*	-0.93*
all	0.10		0.004		2.40		0.0024		0.61*	-0.91*	0.33*	-1.12*	0.36*	-1.13*

Table 2: Significant Pearson correlation coefficients (p<0.05) between the different measured elements per sample type and over all samples types and per fraction. Calculations were performed with log_{10} transformed data.

rainwater

1st fraction

	Al	Si	P	Ca	Mn	Fe
Al						0.82
Si			0.73			

2nd fraction

	Al	Si	P	Ca	Mn	Fe
Al		-0.90				
Si				0.89		
Ca					0.74	

throughfall

1st fraction

	Al	Si	P	Ca	Mn	Fe
orgC	0.98		0.96			0.95
Al			0.71			0.97

trench

1st fraction

	Al	Si	P	Ca	Mn	Fe
orgC			0.61	0.75	0.72	0.73
Al		0.77	0.75	0.75	0.75	0.94
Si				0.84	0.80	0.82
P				0.68	0.69	0.83
Ca					0.98	0.89
Mn						0.88

2nd fraction

	Al	Si	P	Ca	Mn	Fe
Al		0.74		0.56	0.57	0.92
Si				0.67	0.59	0.75
P						0.63
Ca					0.94	0.69
Mn						0.71

3rd fraction

	Al	Si	P	Ca	Mn	Fe
Al		0.75				0.97
Si					0.90	0.82

groundwater

1st fraction

	Al	Si	P	Ca	Mn	Fe
Si				0.79		
P				-0.79		

3rd fraction

	Al	Si	P	Ca	Mn	Fe
Al						0.69
P				-0.65		

stream water

1st fraction

	Al	Si	P	Ca	Mn	Fe
orgC			0.85			
Al						0.60
Si			-0.62	0.78		
P				-0.76		

2nd fraction

	Al	Si	P	Ca	Mn	Fe
Al						0.44
Si			-0.69	0.46		
P				-0.51		

3rd fraction

	Al	Si	P	Ca	Mn	Fe
Al					0.36	0.73
P				-0.53		

all sample types

1st fraction

	Al	Si	P	Ca	Mn	Fe
orgC	0.64	0.53	0.69	0.66	0.64	0.75
Al		0.39	0.40	0.53	0.56	0.89
Si				0.68	0.32	0.40
P					0.47	0.55
Ca					0.33	0.50
Mn						0.68

2nd fraction

	Al	Si	P	Ca	Mn	Fe
orgC					0.69	
Al			0.30		0.33	0.78
Si				0.38		0.32
P				-0.33		0.43
Ca					0.28	0.31
Mn						0.45

3rd fraction

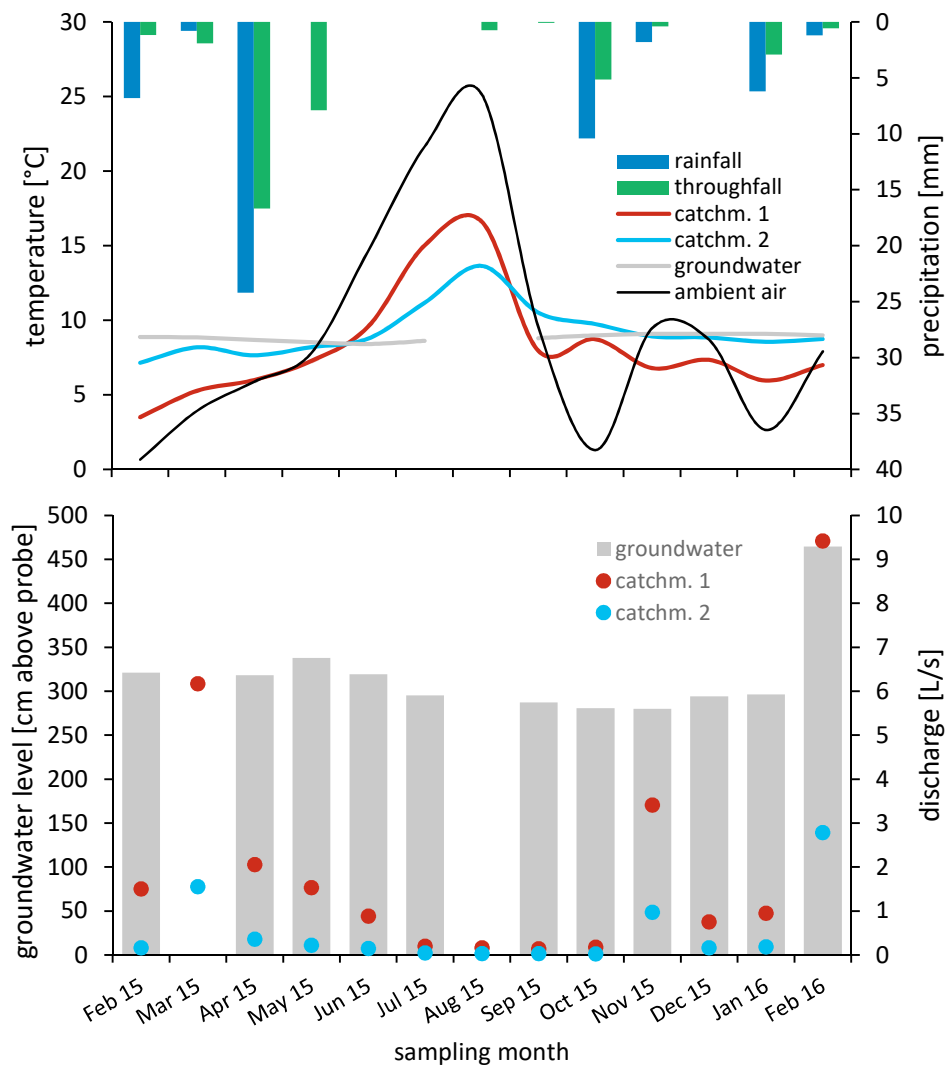|	Al	Si	P	Ca	Mn	Fe
orgC	0.37		0.43			0.38
Al		0.55	0.45		0.40	0.82
Si					0.63	0.58
P				-0.31		0.36
Ca						
Mn						0.45

Figure 1: Hydrological and meteorological parameters recorded during the sampling period. Top: Temperature measured in stream water at both catchments, in groundwater and in the air as well as precipitation above and below tree canopy, Bottom: Average daily discharge at both catchments and groundwater level. Catchm. = catchment.
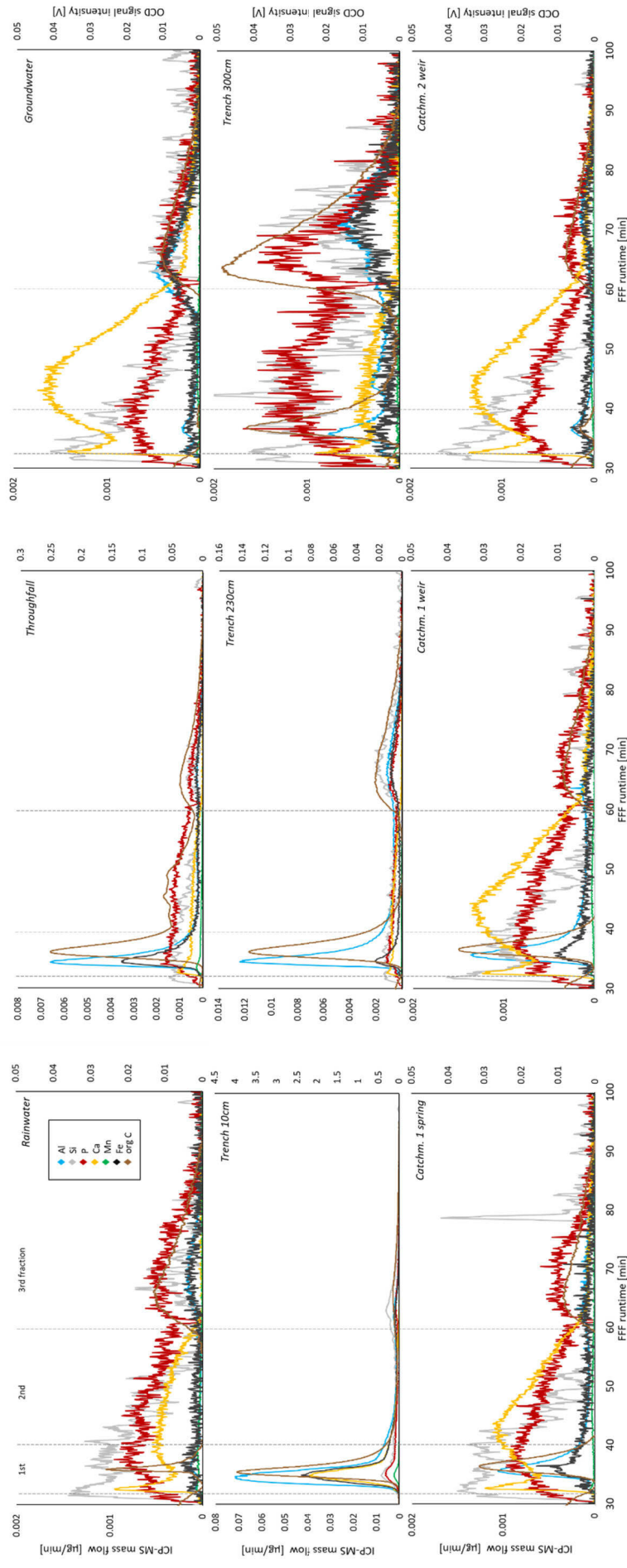
Figure 2: Fractograms of Asymmetric Flow Field Flow Fractionation coupled to ICP-MS and OCD. Data averaged over all samples taken per sample ICP-MS data: drift correction through internal standard Rh and baseline corrected, OCD data: baseline corrected prior to visualization. Note the different scaling of the y-axes. X-axes shortened, thus focus time not shown. Dotted lines separate the different fractions. Catchm. = catchment.
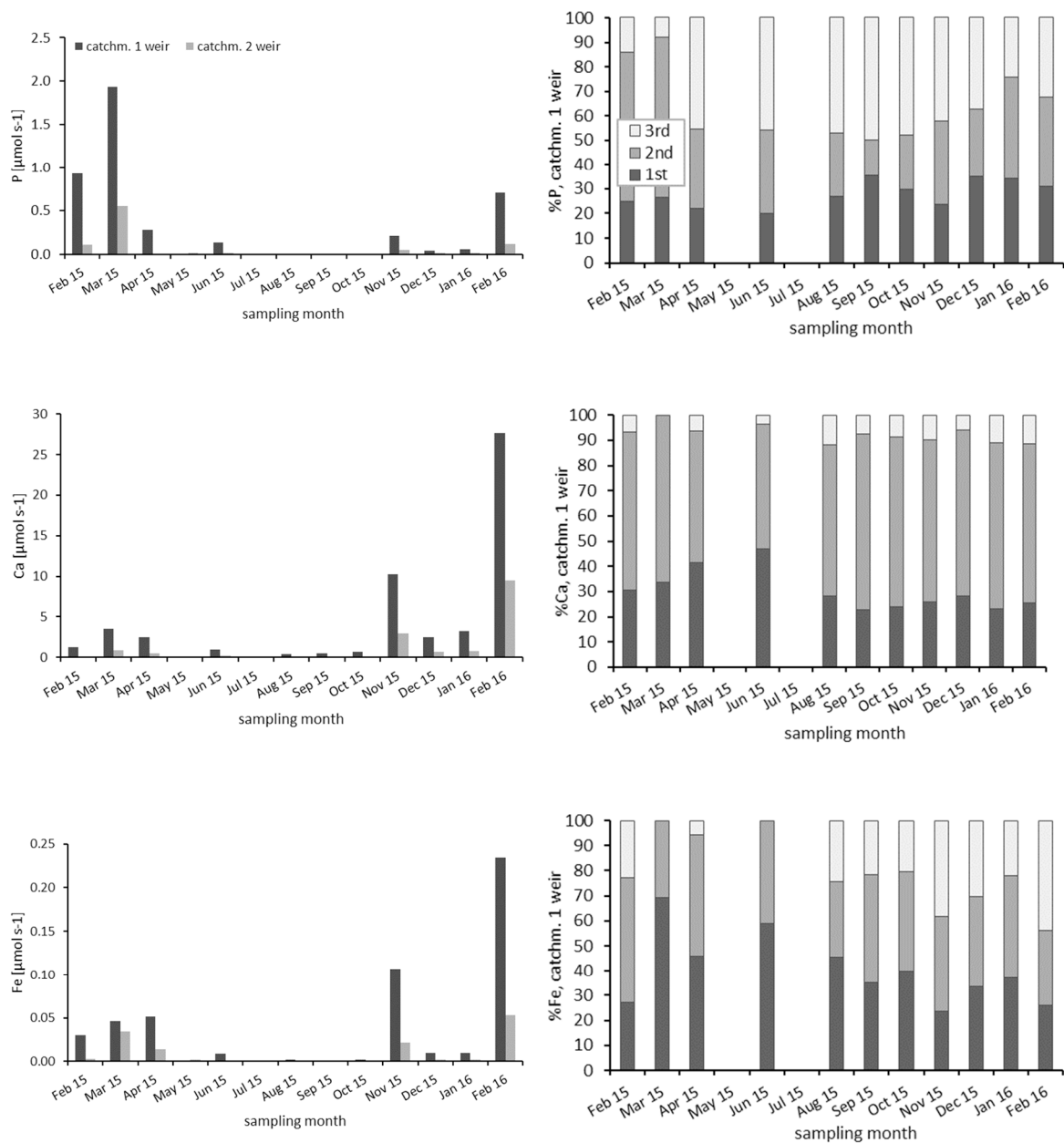
Figure 3: left: All particulate element loads for P, Ca and Fe at both catchments; right: Relative proportions of respective 1st, 2nd and 3rd fraction P, Fe and Ca relative to all colloidal concentrations at catchment 1 weir representative of all sample types. Catchm. = catchment.
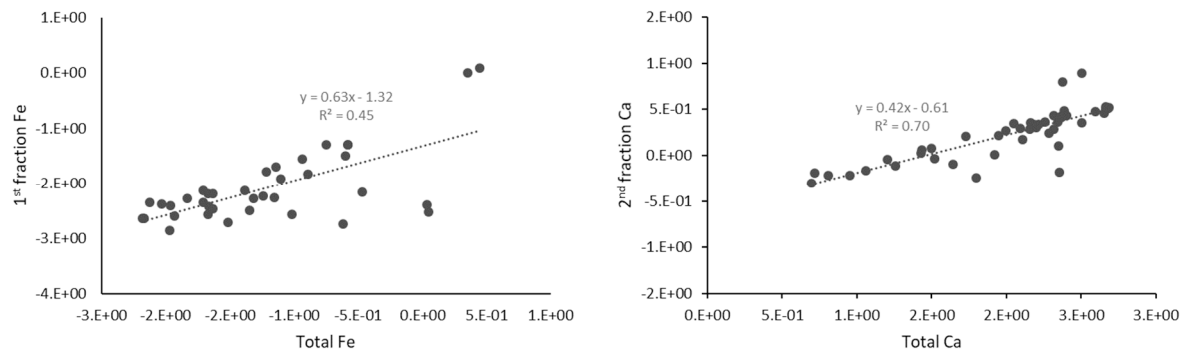
Figure 4: Exemplary relation of colloidal elemental concentration in dependence of total elemental concentrations across all samples taken. Ca and Fe were chosen here to contrast the findings in Gottselig et al. [2017a]. Left: $\log_{10}$ transformed data of 1st fraction Fe in dependence of total Fe, right: $\log_{10}$ transformed data of 2nd fraction Ca in dependence of total Ca. Unit: µmol/L, n = 65. Compare Table 1, top.

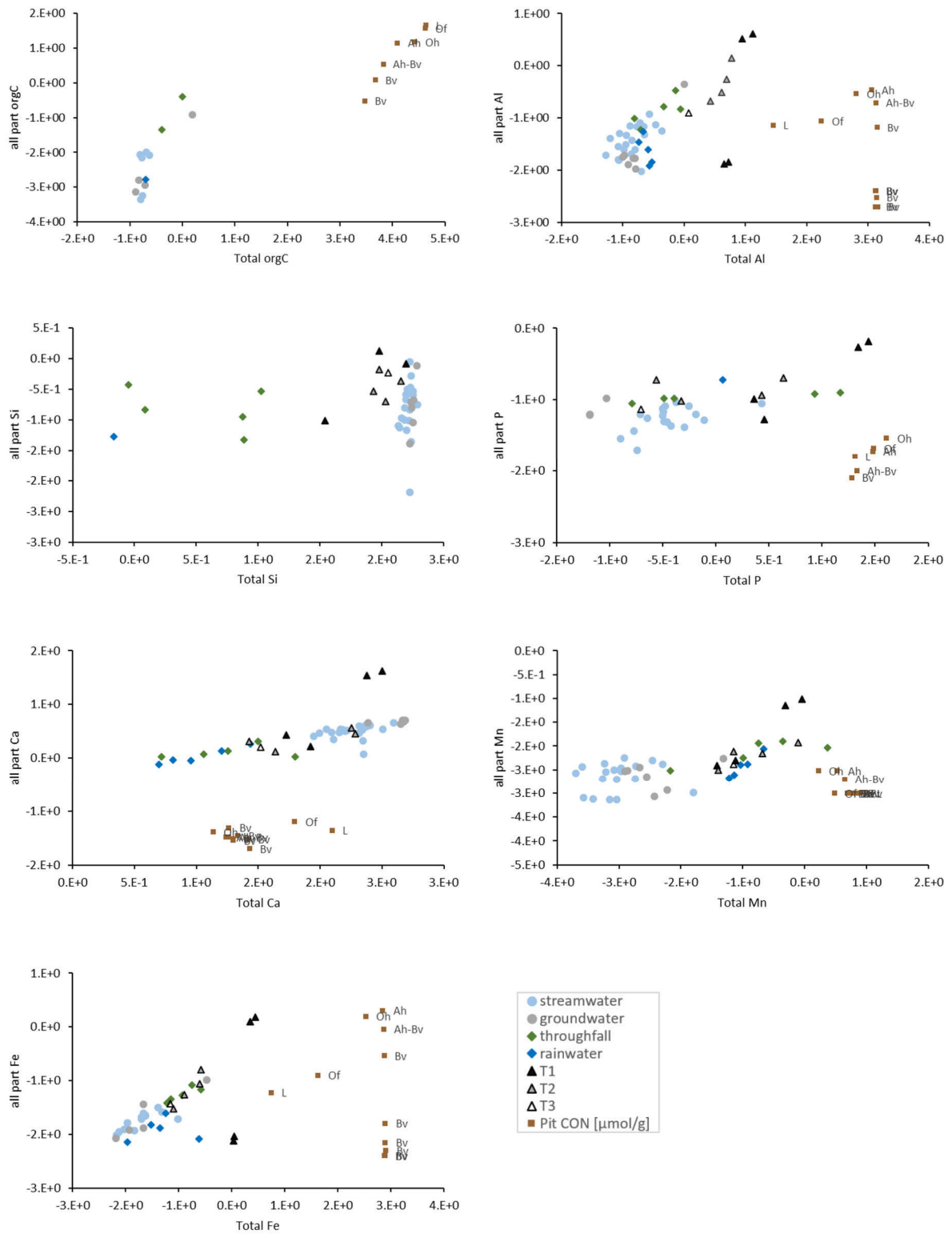Figure 5: Discrimination of sample types in all colloidal vs. total elemental concentration plots. Concentrations of aqueous samples in μmol L^{-1} were log$_{10}$ transformed prior to visualization. Samples of the soil pit were taken in Nov 13, all colloidal concentration data of the water dispersible colloids (WDC) was taken from Missong et al. (2018a) and total concentrations from Lang et al. (2017), both data sets were transferred to the unit μmol g$_{soil}^{-1}$ for better comparison.